Available online at www.sciencedirect.com
ScienceDirect
Trans. Nonferrous Met. Soc. China 29(2019) 2035−2046
Transactions of Nonferrous Metals Society of China
www.tnmsc.cn

Effect of post-weld heat treatment on microstructure and mechanical properties of welded joints of 6061-T6 aluminum alloy

Jie YI[1,2], Guan WANG[2], Shi-kang LI[3], Zhi-wen LIU[4], Yan-li GONG[1]

1. College of Mechanical Engineering, Hunan Industry Polytechnic, Changsha 410208, China;
2. State Key Laboratory of Advanced Design and Manufacturing for Vehicle Body, Hunan University, Changsha 410082, China;
3. Qiuzhen College, Huzhou University, Huzhou 313000, China;
4. College of Mechanical Engineering, University of South China, Hengyang 421001, China

Received 1 January 2019; accepted 15 August 2019

Abstract: 6061 aluminum alloy T-joints were welded by double-pulsed MIG welding process. Then, the post-weld heat treatment was performed on the welded T-joints. The weld microstructure under different aging temperature and time was investigated by transmission electron microscopy and scanning electron microscopy. The mechanical properties were examined by hardness test and tensile test. The results showed that the micro-hardness was sensitive to heat treatment temperature and time. Increasing temperature was beneficial to the shortening of peak aging time. There were a large number of dislocations and few precipitates in the welded joints. With the increase of post-weld heat treatment temperature and time, the density of dislocation decreased. Meanwhile, the strengthening phase precipitated and grew up gradually. When the post-weld heat treatment temperature increased up to 200 °C, large Q' phases were observed. And they were responsible for the peak value of the micro-hardness in the welded joints.

Key words: 6061 aluminum alloy; double-pulsed MIG welding; post-weld heat treatment; microstructure evolution; mechanical property

1 Introduction

Aluminum alloys have many excellent properties, such as low density, high yield stress to tensile strength ratio and excellent corrosion resistance [1−3]. They are widely used in the automotive and railway transportation industry for energy saving and emission reduction. However, the poor weldability of aluminum alloys, such as strong oxidation and thermal conductivity, may lead to many defects of welded joints, for example incomplete fusion, porosity and cracking [4]. Pulsed MIG welding is an efficient and high quality welding method for aluminum alloys with good droplet transfer control capability [5]. Double pulsed MIG welding is developed based on the pulsed MIG welding. During the welding process, the change of the welding current between the thermal pulse and the thermal matrix leads to the diversification of the weld temperature and stress. Therefore, it may lead to a typical corrugated appearance and strong stirring effect of the weld pool, which has a significant influence on the temperature and stress of the weld pool during the welding process. And it would further affect the quality of the welded joint [6,7].

After MIG welding, the strength in some sub-zones (weld zone and heat affected zone) of the welded joint would decrease. Such a strength softening can be restored to a certain extent in subsequent aging treatment. Aging treatment could promote the precipitation in the weld zone and make the structure and chemical composition more uniform [8,9]. And then it also could improve the mechanical properties of the welding joint. The post-weld heat treatment process of 6061 aluminum alloy was studied by AHMAD and BAKAR [10]. It was found that MIG welding can effectively improve the microstructure and mechanical

Foundation item: Projects (2019JJ70077, 2019JJ50510) supported by the National Science Foundation of Hunan Province, China; Project (31665004) supported by Open Fund of State Key Laboratory of Advanced Design and Manufacture for Vehicle Body, China; Projects (18B552, 18B285) supported by Scientific Research Fund of Hunan Provincial Education Department, China
Corresponding author: Shi-kang LI, Tel: +86-15874071655, E-mail: kangkangli2009@126.com;
Zhi-wen LIU, Tel: +86-734-8578031, E-mail: liuzhiwen1008@163.com
DOI: 10.1016/S1003-6326(19)65110-1

properties of the welded joint. RAO et al [11] studied the effect of welding process, heat treatment and filler materials on the cracking tendency in the welding zone of 6061 aluminum alloy. MUOZ et al [12] found that the hardness of the joint welded by MIG was increased by nearly 50 MPa of Al−4.5Mg−0.26Sc alloy after the post-weld heat treatment under 300 °C for 1 h. CERRI and LEO [13] studied the effect of post-welding-heat treatments on the microstructure and mechanical properties of double lap FSW joints. During exposure at 200 and 300 °C, the tensile strengths and micro-hardness in the nugget center slightly decreased with the increase of time and temperature. GÜRAL et al [14] found that the microstructure of 1010 steel welded under controlled atmosphere of argon was particularly more homogeneous after intermediate quenching treatment. JEON et al [15] studied the tensile behavior of an as-welded Nimonic 263 specimen at room temperature and 1053 K. With increasing resolutionization time, the YS and UTS tended to decrease along with the increase in tensile ductility.

Post-weld heat treatment was usually carried out to improve the strength and hardness of welded joints after welding. In this study, 6061 aluminum alloy T-joints were welded by double pulsed MIG welding. The effects of single-stage artificial aging heat treatment on mechanical properties and microstructure of the welding joints were systematically studied by means of hardness testing and microstructure observation. The research results will provide guidance for the formulation of heat treatment process for aluminium alloy welded joints.

2 Experimental

The base material under study was a 2 mm-thick 6061-T6 Al alloy sheet and the filler wire adopted was ER5356 Al−Mg alloy with a diameter of 1.2 mm. The chemical compositions of the base metal are given in Table 1. Welding operation in this work was fully done by an automatic MIG welder at the self-made fixture. The welding power source used was DP400 developed by OTC to provide DP-MIG.

Table 1 Chemical composition of 6061-T6 alloy (wt.%)

Mg	Si	Fe	Cu	
0.8−1.2	0.4−0.8	0.70	0.15−0.4	
Cr	Mn	Zn	Ti	Al
0.04−0.3	0.15	0.25	0.15	Bal.

Figure 1 shows the schematic diagram of the T-joint. The dimensions of the web and the flange were 200 mm × 50 mm and 200 mm × 80 mm, respectively. During the welding process, the arc was welded in the *X* direction on one side.

In order to investigate the effect of welding parameters on the mechanical properties of the welded joints, hardness tests were carried out. Hardness measurements on the upper surfaces of polished samples were conducted on a HXD−1000T Vickers hardness testing machine under a load of 4.9 N and a duration time of 10 s. In order to study the tensile properties of the alloy under different aging treatments, ambient uniaxial tensile test was carried out on an Instron 3369 electrical testing machine. Test parameters were also defined according to ASTM: E8-M-04 standard; the tensile speed was set as 2 mm/min. The tensile test sample and dimensions of the tensile test sample are shown in Fig. 2.

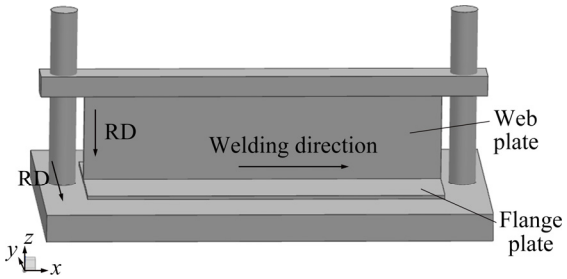

Fig. 1 Schematic diagram of T-joint

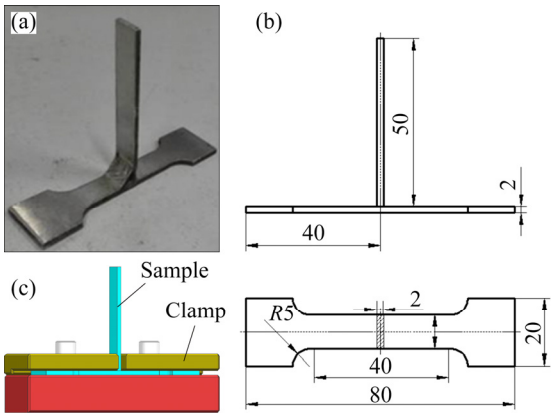

Fig. 2 Tensile test sample (a) and its dimensions (b), and clamping apparatus for tensile tests (c) (unit: mm)

The metallographic structure and precipitate morphology of the cross-section of welded joints were observed by means of transmission electron microscopy (TEM) and high resolution TEM (HRTEM). Specimens for TEM were slowly sliced perpendicularly to the seam to about 2 mm in thickness by wire cut electrical discharge machining from different subzones of the joint, i.e., the base metal, the weld toe (namely the fusion line), the HAZ zones. All these specimens were first mechanically ground to about 100 μm in thickness and then further thinned by twin-jet electro-polishing with a solution of 25 vol.% nitric acid and 75 vol.% methanol at −25 °C, 18 V and 40 mA. TEM observations were

performed on a Tecnai F20 TEM system (FEI, Hillsboro, OR, USA) operated at 200 kV.

3 Results and discussion

3.1 Aging hardening behavior

The hardness of the welding zone increased with the increase post-weld heat treatment time and temperature, as shown in Fig. 3. After reaching the peak value, hardness in the welding zone entered a stable stage. It can be seen that there was a remarkable difference of aging hardening at different aging temperatures. And the time reaching the peak value of the hardness shortened with the increase aging temperature. At the same time, the peak hardness increased until the temperature reached up to 200 °C. At the aging temperatures of 160, 180 and 200 °C, the time corresponding the peak hardness was 12, 8 and 4 h, respectively. And the peak hardness values were HV 76, HV 84 and HV 82, respectively. The above results showed that the precipitation hardening process in the welding zone depended on the post-weld heat treatment time and temperature. The whole precipitation process was carried out by the diffusion of the solute atoms in aluminum matrix. The diffusion coefficient (D) is a measure of the mobility of the diffusing species, which is related to the temperature, and can be written as

$$D = D_0 \exp(-\frac{Q}{RT}) \quad (1)$$

where D_0 is the diffusivity constant, Q is the activation energy for diffusion, T is the temperature, R is the gas constant (8.31 J/(K·mol)).

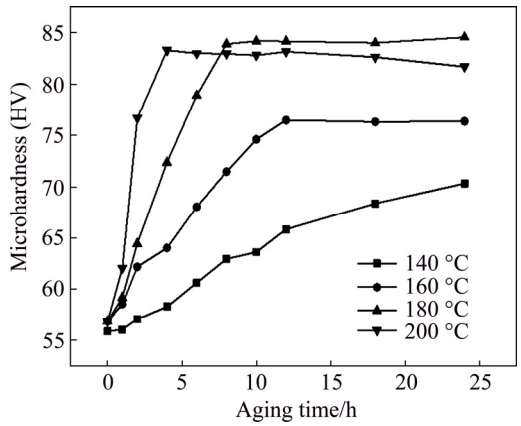

Fig. 3 Varation of microhardness of joint at different post-weld heat treatment temperatures

It can be seen from Eq. (1) that the diffusion coefficient increased exponentially with the increase of temperature. Therefore, the temperature has a great influence on the whole diffusion process. Increasing the heat treatment temperature would greatly increase the diffusion coefficient, leading to accelerating the diffusion process of the solute atoms. Thus, the time for the peak aging was shortened. However, the precipitation hindering the dislocation movement tended to aggregate and coarsen as the temperature increased, resulting in the decrease of the mechanical properties. The peak hardness decreased from HV 84 at the temperature of 180 °C to HV 82 at the temperature of 200 °C. The peak aging hardening was not achieved at 140 °C for 24 h. This was mainly due to the fact that decreasing the aging temperature would greatly reduce the diffusion rate and thus influence the precipitation. Therefore, the time for peak aging would be longer at lower temperature. The highest hardness was HV 84 at 180 °C, as shown in Fig. 3. Thus, the optimum aging process for obtaining the highest mechanical property of 6061 aluminum alloy welds was aged at 180 °C for 8 h.

Figure 4 shows the hardness of the weldment. It can be seen that the hardness in the welding zone increased with the increase of heat treatment temperature and time. After heat treatment at 180 and 200 °C, the highest hardness values in the welding zone were HV 84 and HV 82, respectively. The hardness in the welding zone was far lower than that in the matrix zone.

With the increase of heat treatment time, the hardness in the welding zone increased and reached stable stage after aging for 1 h. The supersaturated solid solution state near the welding zone was obtained due to the high thermal cycling temperature. Thus, the hardness near the welding zone increased with the increasing aging time. The peak hardness values at 140, 160, 180 and 200 °C were HV 94, HV 95, HV 94 and HV 96, respectively. Mg and Si solute precipitates from the supersaturated solid solution and forms fine dispersed phase in the aging process of Al−Mg−Si aluminum alloy [16−18]. The two important parameters affecting the precipitation behavior were temperature and time in the same alloy [19]. In the aging process, controlling the heat treatment temperature and time could improve the structure, quantity, size and distribution of secondary phase and the mechanical property of the alloy [20−22]. Therefore, it is important to establish a reasonable aging process to improve the mechanical property of aluminum alloy.

3.2 Effect of aging processing on microstructure

According to the results of the hardness, it can be seen that the weakest zone of the welded joints was located in the heat affected zone. In order to further study the microstructure of the heat affected zone, TEM was used to characterize the microstructure of the welding zone without post heat treatment and the softening zone after post-weld heat treatment at different temperatures.

Figure 5 shows the TEM field image and electron

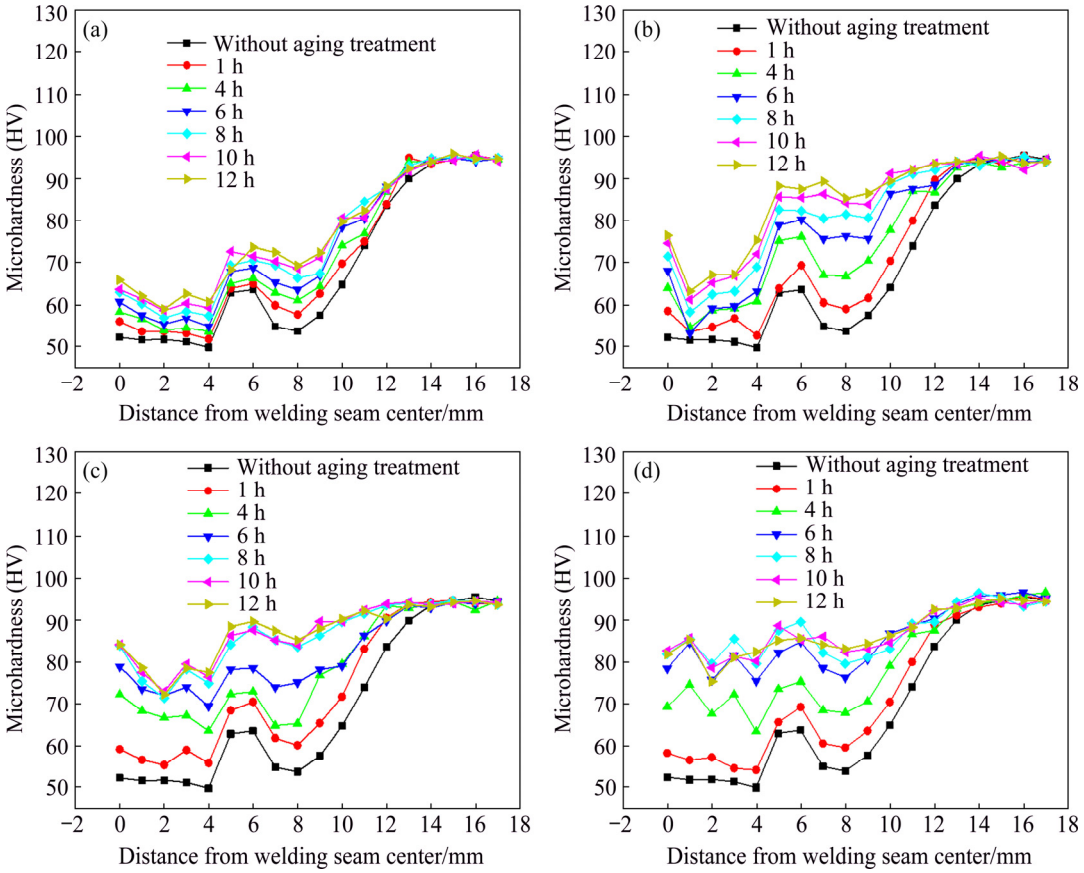

Fig. 4 Microhardness of joint at different post-weld heat treatment temperatures: (a) 140 °C; (b) 160 °C; (c) 180 °C; (d) 200 °C

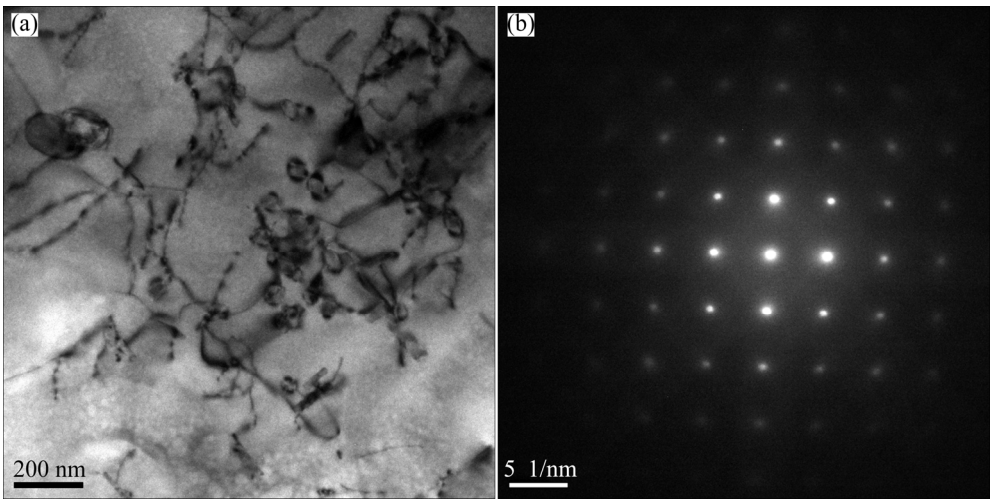

Fig. 5 TEM image (a) and diffraction pattern (b) of joint under $[001]_{Al}$ zone axis in welding zone without heat treatment

diffraction pattern in the welding zone without post-weld heat treatment. There were a large number of dislocations in the welding zone, and no precipitation was observed, as shown in Fig. 5(a). Based on the electron diffraction, as shown in Fig. 5(b), there were only diffraction spots of aluminum matrix, which also indicated that there was no precipitation in the welding zone. From the results of TEM, it can be concluded that the precipitation completely redissolved into the aluminum matrix at the effect of high temperature welding cycle, leading to a significant decline of the mechanical properties. In addition, there were a large number of dislocations in the matrix. This was because that there was no enough time to make the dislocations completely degenerate during the rapid welding process.

Figure 6 shows the bright field image and the high-resolution of TEM in the softening zone after post-weld heat treatment at 140 °C for 24 h. There were a large

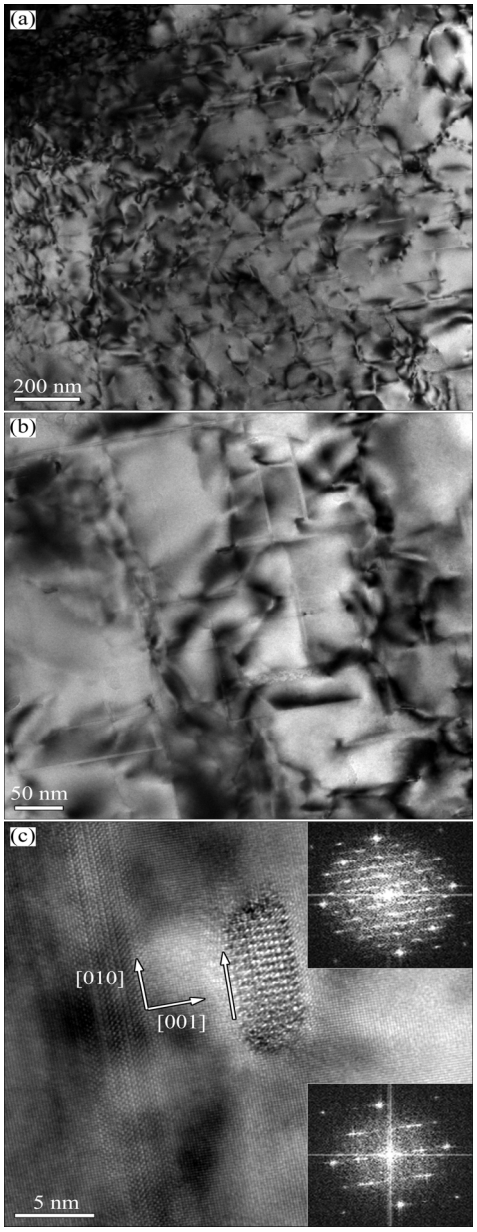

Fig. 6 Microstructures of softening zone after post-weld heat treatment at 140 °C for 24 h: (a, b) TEM images; (c) HRTEM image

number of dislocations in the matrix zone, and the amount of dislocations did not decrease compared with that in the matrix without post-weld heat treatment. This was due to the low temperature of 140 °C, which cannot make the dislocations recover and degenerate. However, it can be clearly seen that there were precipitations after heat treatment at 140 °C and the length of the precipitation was about 100 nm, as shown in Fig. 6(b). High resolution observations were performed on the precipitation, as shown in Fig. 6(c). It was found that the precipitation grew along the [100] direction of the aluminum matrix, and its Fourier transform was inset in Fig. 6(c). According to Refs. [23−25], the precipitation may be *L*/*Q* phase.

Figure 7 shows the bright field and high resolution images of the softening zone after aging at 160 °C for 12 h. It can be seen that there were still a few dislocations in the matrix zone. But the degradation of the dislocations was more serious than that without heat treatment or aging at 140 °C for 24 h. This indicated that there were enough energy at 160 °C for the recovery and degeneration of dislocations. Lath-shaped and needle-shaped phases were observed after aging at 160 °C for 12 h, as shown in Fig. 7(b). High resolutions of the phases were performed, as shown in Fig. 7(c). Lath-shaped phase grew along the [100] direction of the aluminum matrix. According to Refs. [23−25], the precipitation may be *L*/*Q* phase. The needle-shaped

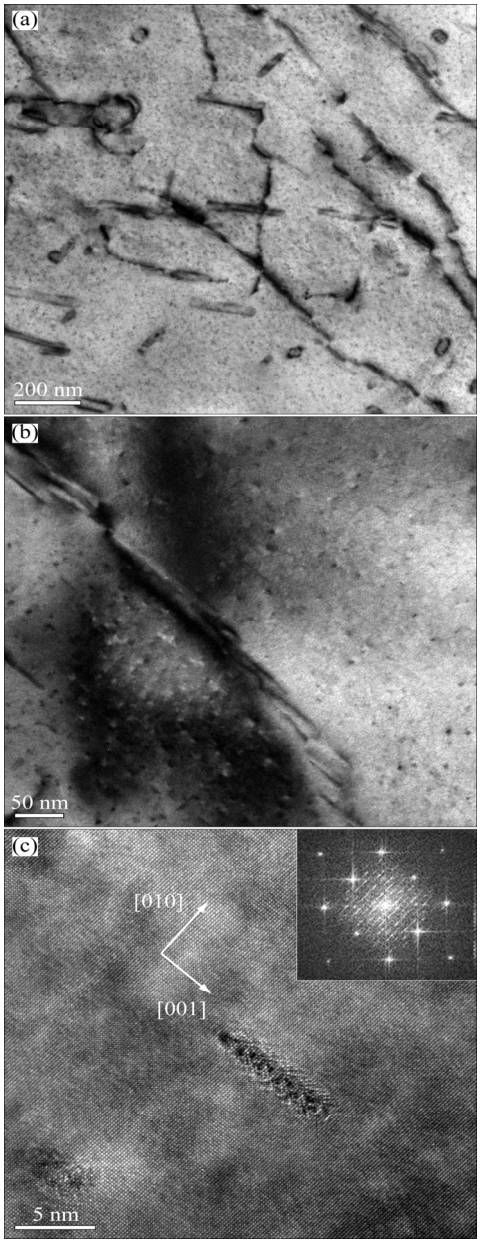

Fig. 7 Microstructures of softening zone after post-weld heat treatment at 160 °C for 12 h: (a, b) TEM images; (c) HRTEM image

phases were completely coherent with the aluminum matrix, as shown in Fig. 7(c).

Figure 8 shows the bright field and high resolution images of the softening zone after aging at 180 °C for 8 h. As shown in Fig. 8(a), there were also a few dislocations in the matrix zone and the degradation of the dislocations was more serious. It can be seen that the size of the precipitation was much larger than that in the softening zone after aging at 160 °C, as shown in Fig. 8(b). High resolutions of the phases were performed, as shown in Fig. 8(c). The precipitation grew along the [510] direction of the aluminum matrix. According to Refs. [23−25], the precipitation may be Q' phase. Simultaneously, there were much larger number and bigger size of β phases.

Figure 9 shows the bright field TEM and high resolution images of the softening zone after aging at 200 °C for 4 h. As can be seen from Fig. 9(a), there were a few number of dislocations in the matrix zone. Most of the dislocations have been degenerated during heat treatment, which was similar to the softening zone after heat treatment at 180 °C for 8 h. The size of precipitation after aging at 200 °C for 4 h was bigger than that in the softening zone after aging at 180 °C for 8 h. High resolutions of the phases were performed, as shown in

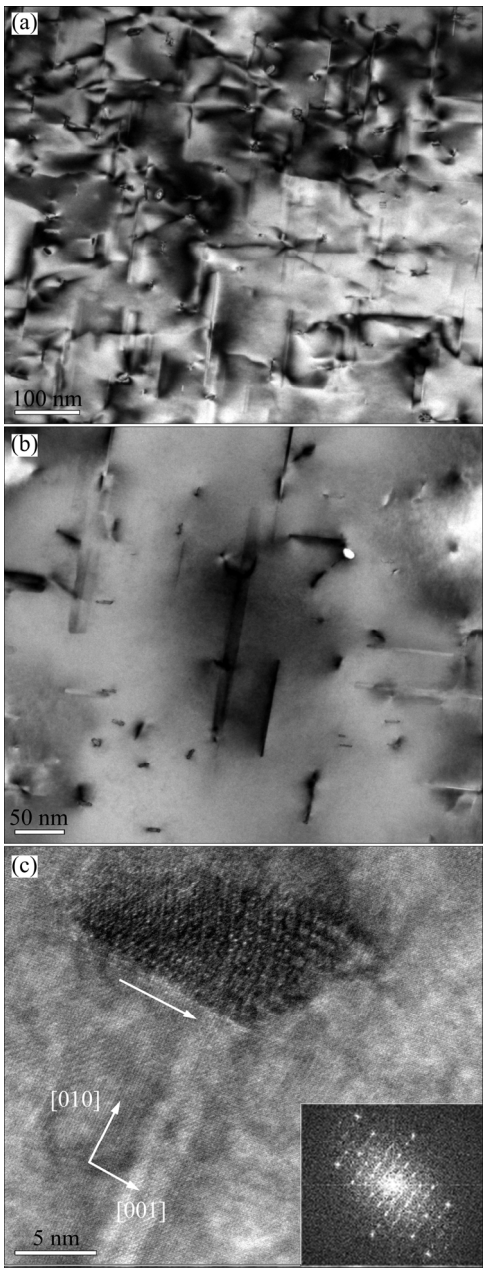

Fig. 8 Microstructures of softening zone after post-weld heat treatment at 180 °C for 8 h: (a, b) TEM images; (c) HRTEM image

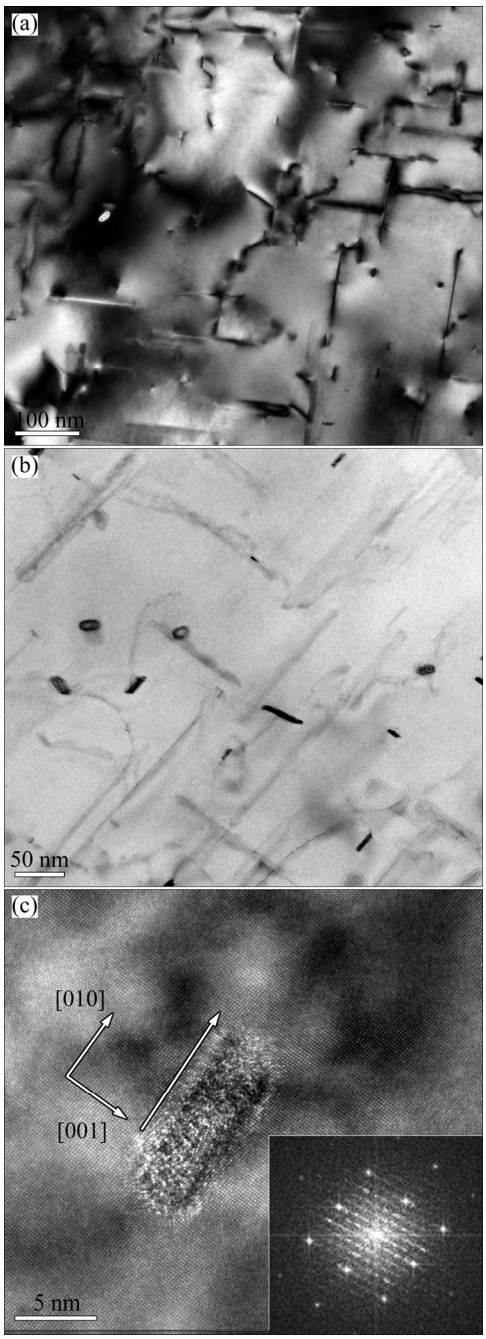

Fig. 9 Microstructures of softening zone after post-weld heat treatment at 200 °C for 4 h: (a, b) TEM images; (c) HRTEM image

Fig. 9(c), and found that the precipitation grew along the [150] direction of the aluminum matrix. According to Refs. [23−25], the precipitation may be Q' phase. At the same time, the number of the precipitation was larger and the size was bigger.

According to above analysis, the microstructure evolution at different temperatures was mainly reflected by two aspects: the precipitation evolution and the dislocation evolution. There were a large number of dislocations in the welded parts. Although the welding zone was affected by the welding thermal cycle during welding process, the dislocations did not change significantly because of the short duration of the welding heat. That is to say, the dislocations containing in the base metal were still stored in the matrix. With the increase of post-weld heat treatment temperature, the number of dislocations decreased. At the post-weld heat treatment temperature of 140 °C, the number of dislocations did not change significantly. However, the number of dislocations decreased significantly after post-weld heat treatment at 160 and 180 °C. After the post-weld heat treatment at 160 °C, the dislocations almost disappeared.

There was no precipitates in the welding zone after welding process. This indicated that the precipitates existing in the base metal could be dissolved back into the matrix due to the influence of welding heat during the welding process. During the post-weld heat treatment at different temperatures, the secondary phase precipitated continuously with the decrease of dislocations and the size of secondary phase increased with the increase of heat temperature. Some lath-like L/Q'' phases precipitated after heat treatment at 140 °C for 24 h. After heat treatment at 160 °C for 12 h, there were not only the L/Q'' phases, but also small size, needle-like phases were observed. The needle-like phases were coherent with the matrix. During the heat treatment at 180 °C for 8 h, the number of the dislocations decreased and the precipitations grew up, forming the larger Q' phase. Increasing the heat treatment temperature up to 200 °C, the dislocations completely disappeared and the precipitation was mainly the Q' phase. The size of the precipitation was bigger than that heat treated at 180 °C for 8 h. The profiles after heat treatment at 200 °C for 4 h exhibited the highest micro-hardness, which was attributed to the precipitation of the Q' phase.

3.3 Mechanical properties

By means of uniaxial tensile tests at ambient temperature, the engineering stress versus displacement curves for the specimens under different heat treatment conditions were obtained, as shown in Fig. 10. It can be seen that the welded alloy exhibited poor tensile properties. The engineering stress was only 157 MPa. After heat treatment, the engineering stress of the welded joints improves considerably with limited increase of the elongation. As aging temperature extended, the engineering stress and elongation increased. This result indicates that the aging heat treatment was beneficial to improving engineering stress of the welded joints. However, the engineering stress increased with the aging temperature increasing to 200 °C, while the elongation declined. The welded joints aged at 180 °C for 8 h exhibit high tensile strength and elongation. As we know, keeping large ductility at the high strength can result in a significant increase in toughness [26,27]. Therefore, the welded joints aged at 180 °C for 8 h can better cover the needs for high damage tolerance and high durability industry.

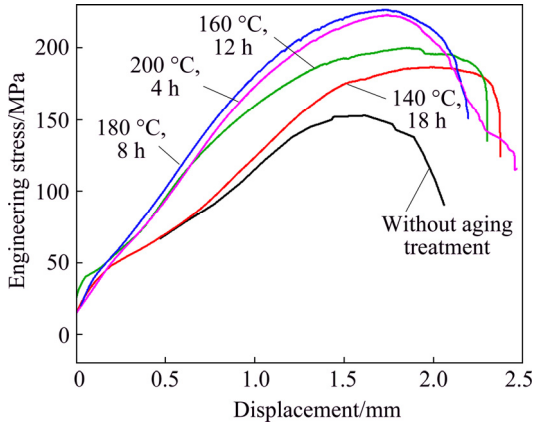

Fig. 10 Ambient uniaxial tensile stress−displacement curves of welded alloy at different heat treatment temperatures

3.4 Fracture morphology

Figure 11 shows the fracture morphologies of tensile specimens of the welded alloy without heat treatment. In the low magnification image presented in Fig. 11(a), the fractured cross section exhibits a planar area. The fracture surfaces of the tensile specimens are relatively smooth and have a lot of dimples with different sizes and depths on the upper surface. The average diameter of the dimples was approximately 10 μm, as shown in Figs. 11(c) and (d). These shallow and small dimples correspond to the inferior ductility of the welded joint. While the river pattern fracture surface which indicated the brittle fracture was observed on the bottom surface. According to the fracture surface, it can be seen that the crack may originate from the upper surface of the tensile sample. After a relatively strong plastic deformation, the crack extended to the center of the fracture surface through the dimples, and finally led to the fracture of the tensile sample by brittle fracture.

A detailed view of the fracture surface morphology analyzed by scanning electron microscopy is presented in Fig. 12 for a sample aged at 140 °C for 24 h. In the low

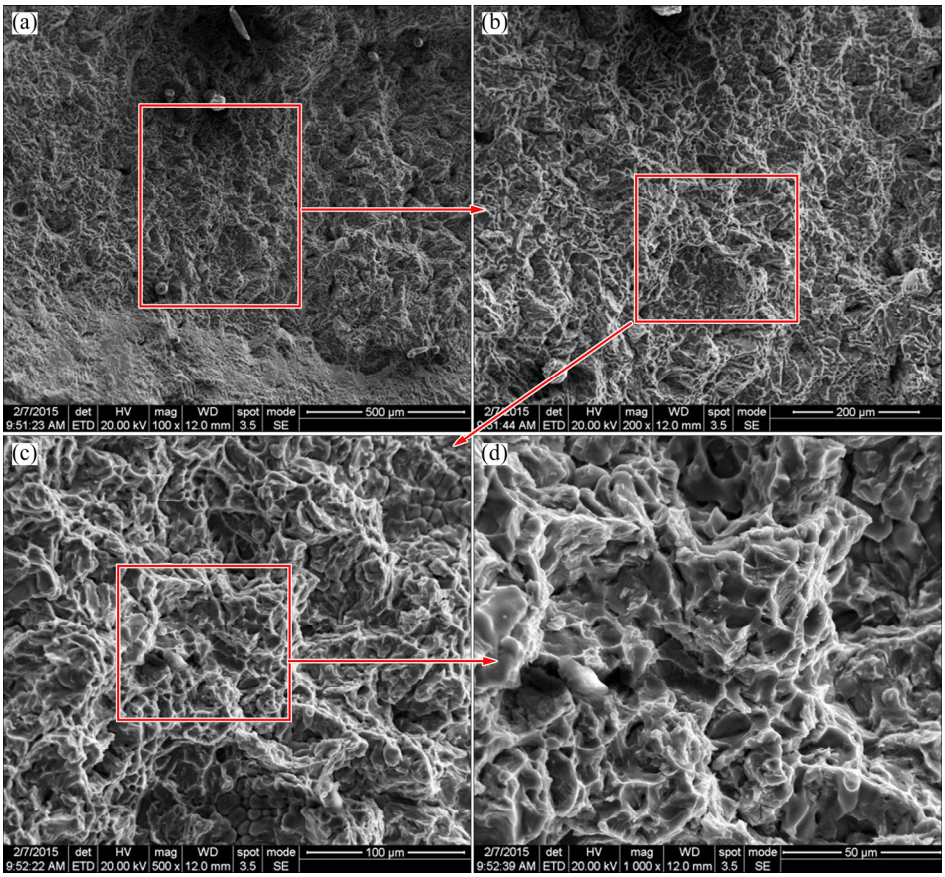

Fig. 11 Tensile fracture morphologies of welded sample without aging treatment

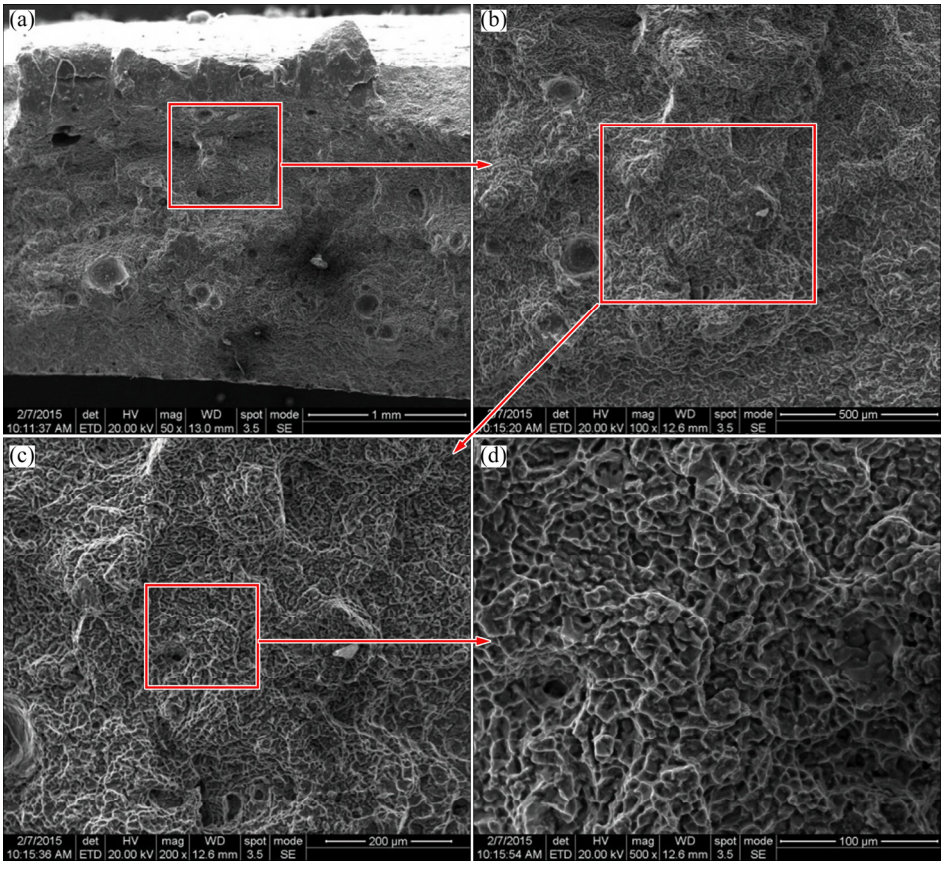

Fig. 12 Tensile fracture morphologies of sample aged at 140 °C for 24 h

magnification image presented in Fig. 12(a), the fracture surfaces of the tensile specimens are unsmooth and shear crack characteristics was observed. Closer inspection inside the fracture surface, there existed uniform rip edges and equiaxed dimples, which indicated that a large plastic deformation was achieved during the process of tensile due to the high energy characteristics of shear crack and rip edge. The average diameter of the dimples was approximately 10 μm, as shown in Figs. 12(c) and (d). Compared with the fracture morphology of the sample without aging, the fracture morphology of the sample aged at 140 °C for 24 h was more uniform, which showed that recrystallization might occur in this alloy at this aging treatment.

For the sample aged at 160 °C for 12 h, the fracture morphology is shown in Fig. 13. In the low magnification image presented in Fig. 13(a), the fracture surfaces of the tensile specimens are unsmooth and a fairly wide range of dimple sizes covers this surface. The diameters of the shallow dimple ranged from 10 to 30 μm. Closer inspection inside the fracture surface, there was no rip edge, which indicated the low yield strength, as shown in Figs. 13(c) and (d).

Figure 14 shows the fracture morphology of the tensile sample aged at 180 °C for 8 h. In the low magnification image presented in Fig. 14(a), the fracture morphology exhibited a markedly different fracture surface morphology in comparison to the fracture morphologies shown in Figs. 11−13. The fracture surface of the tensile specimens at 180 °C for 8 h was relatively smooth. The typical intergranular fracture characteristic was observed, as shown in Fig. 14(d). This intergranular character was also observed in the fracture morphology of the tensile sample aged at 200 °C for 4 h in Fig. 15(d). However, a clear distinction in high magnification fracture morphologies can be found, as shown in Figs. 14(d) and 15(d). There are a number of fine and shallow dimples covering the intergranular fracture surfaces of the tensile sample aged at 200 °C for 4 h (Fig. 15(d)), while the fracture surface of the tensile specimens aged at 180 °C for 8 h is very smooth (Fig. 14(d)). This distinction is mainly attributed to the different grain boundary microstructures in two aging conditions. According to the study of WANG et al [27], the precipitate free zone as well as the continuous and coarse grain boundary precipitates weakens the grain boundary and leads to the intergranular fracture with smooth surfaces under the treatment of T6. For the over-aged specimen, micro-voids nucleate primarily at the discontinuous and coarse grain boundary precipitates during tensile test, and then grow and coalesce within the wide precipitate free zone, which form the fine and

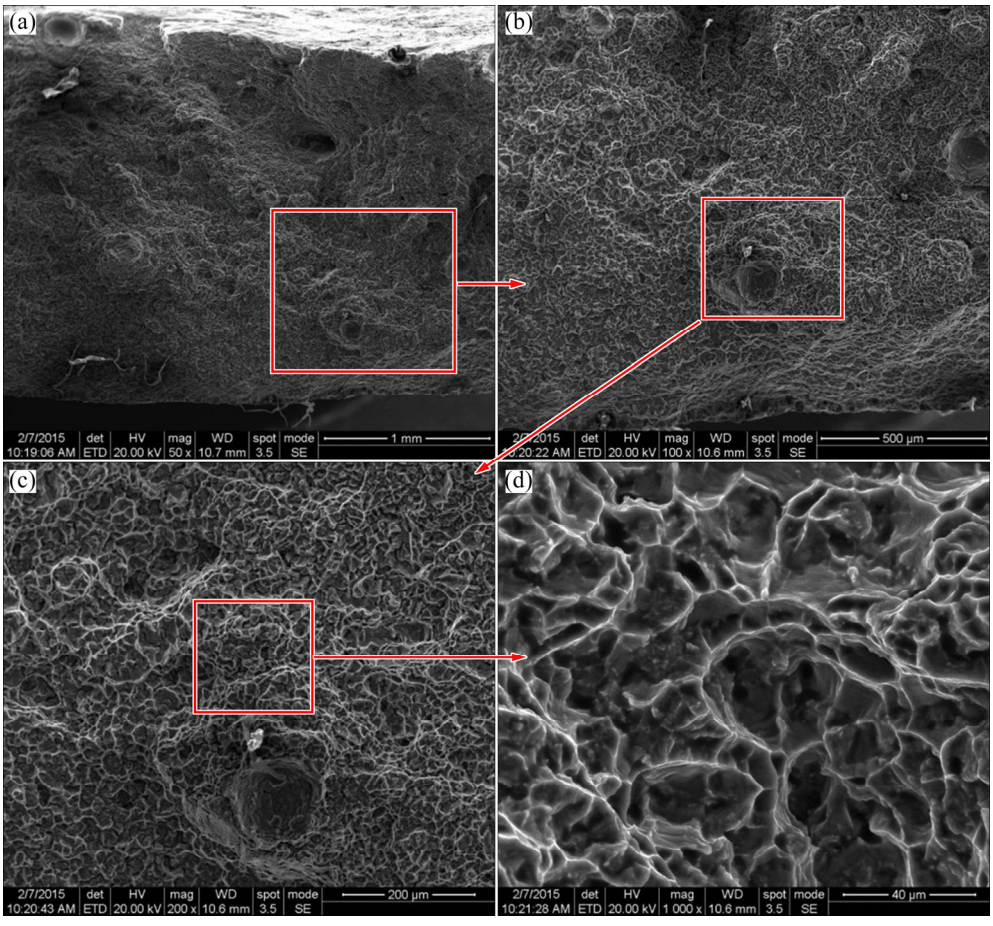

Fig. 13 Tensile fracture morphologies of sample aged at 160 °C for 12 h

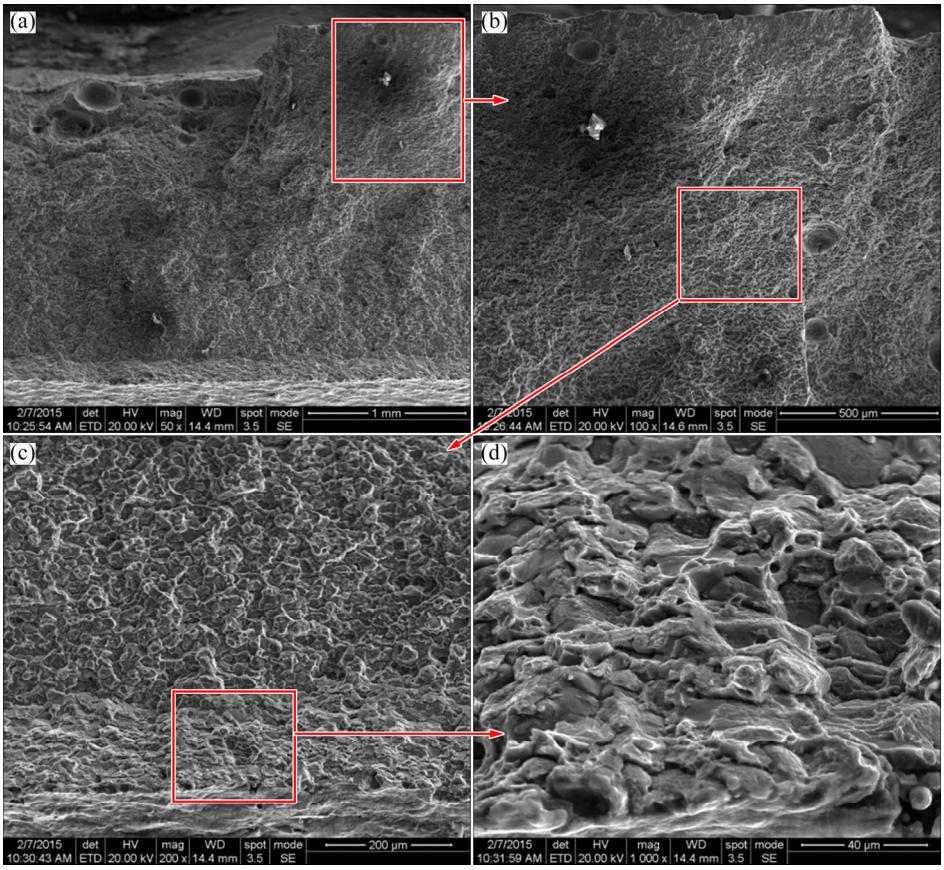

Fig. 14 Tensile fracture morphologies of sample aged at 180 °C for 8 h

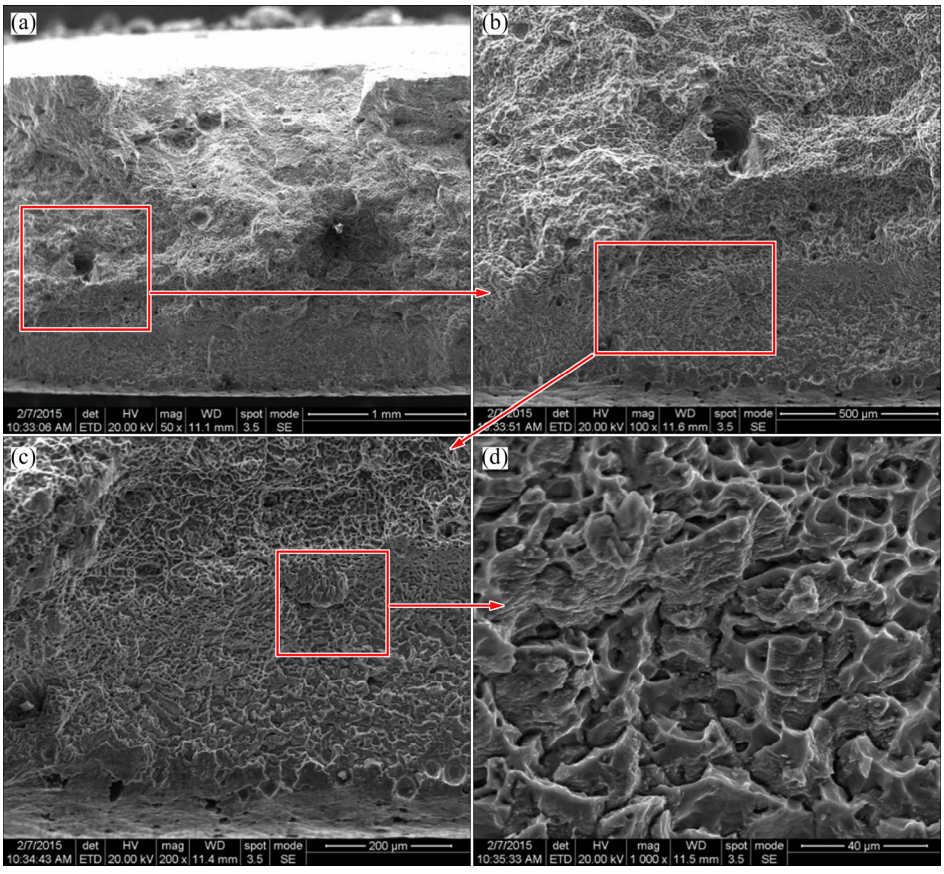

Fig. 15 Tensile fracture morphologies of sample aged at 200 °C for 4 h

shallow dimples covering intergranular fracture surface. It can be seen from the above analyses that aging heat treatment has significant influences on the microstructure and mechanical properties of the welded joints.

4 Conclusions

(1) In the aging heat treatment process, the micro-hardness is sensitive to post-weld heat treatment temperature and time. Increasing temperature is beneficial to the shortening of peak aging time.

(2) The mechanical properties of the welded joints are greatly improved after heat treatment due to precipitates. The profiles after heat treatment at 200 °C for 4 h exhibit the highest micro-hardness, which is attributed to the precipitation of the Q' phase.

(3) In the welded joints without heat treatment, there are a lot of dislocations and few precipitations in the welding zones because of the short duration of the welding heat. With the increase of post-weld heat treatment temperature and aging time, the density of the dislocation in the heat affected zone decreases.

References

[1] LIU L, WU Y X, GONG H, WANG K. Modification of constitutive model and evolution of activation energy on 2219 aluminum alloy during warm deformation process [J]. Transactions of Nonferrous Metals Society of China, 2019, 29(3): 448−459.

[2] LIU Z W, LI L X, LI S K, YI J, WANG G. Entrance shape design of spread extrusion die for large-scale aluminum panel [J]. The International Journal of Advanced Manufacturing Technology, 2019, 101(5−8): 1725−1740.

[3] LIU Z W, LI L X, LI S K, YI J, WANG G. Simulation analysis of porthole die extrusion process and die structure modifications for an aluminum profile with high length–width ratio and small cavity [J]. Materials, 2018, 11(9): 1517−1536.

[4] YI J, ZHANG J M, CAO S F, GUO P C. Effect of welding sequence on residual stress and deformation of 6061-T6 aluminium alloy automobile component [J]. Transactions of Nonferrous Metals Society of China, 2019, 29(2): 287−295.

[5] WU K Y, YIN T, DING N, ZENG M, LIANG Z Y. Effect of phase on the behavior of metal transfer in double-wire pulsed GMAW [J]. The International Journal of Advanced Manufacturing Technology, 2018, 97(9−12): 3777−3789.

[6] MESEGUER-VALDENEBRO J L, PORTOLES A, MATÍNEZ-CONESA E. Electrical parameters optimisation on welding geometry in the 6063-T alloy using the Taguchi methods [J]. The International Journal of Advanced Manufacturing Technology, 2018, 98(9−12): 2449−2460.

[7] ZHAN X H, WU Y F, KANG Y, LIU X, CHEN X D. Simulated and experimental studies of laser-MIG hybrid welding for plate-pipe dissimilar steel [J]. The International Journal of Advanced Manufacturing Technology, 2019, 101(5−8): 1611−1622.

[8] SAFARBALI B, SHAMANIAN M, ESLAMI A. Effect of post-weld heat treatment on joint properties of dissimilar friction stir welded 2024-T4 and 7075-T6 aluminum alloys [J]. Transactions of Nonferrous Metals Society of China, 2018, 28(7): 1287−1297.

[9] OZER G, KARAASLAN A. Properties of AA7075 aluminum alloy in aging and retrogression and reaging process [J]. Transactions of Nonferrous Metals Society of China, 2017, 27(11): 2357−2362.

[10] AHMAD R, BAKAR M A. Effect of a post-weld heat treatment on the mechanical and microstructure properties of AA6061 joints welded by the gas metal arc welding cold metal transfer method [J]. Materials and Design, 2011, 32(10): 5120−5126.

[11] RAO K P, RAMANAIAH N, VISWANATHAN N. Partially melted zone cracking in AA6061 welds [J]. Materials and Design, 2008, 29(1): 179−186.

[12] MUNOZ A C, RUCKERTET G, HUNEAU B, SAUVAGE X, MARYA S. Comparison of TIG welded and friction stir welded Al−4.5Mg−0.26Sc alloy [J]. Journal of Materials Processing Technology, 2008, 197(1): 337−343.

[13] CERRI E, LEO P. Mechanical properties evolution during post-welding-heat treatments of double-lap Friction stir welded joints [J]. Materials and Design, 2011, 32(6): 3465−3475.

[14] GÜRAL A, BOSTAN B, OOZDEMIR A T. Heat treatment in two phase region and its effect on microstructure and mechanical strength after welding of a low carbon steel [J]. Materials and Design, 2007, 28(3): 897−903.

[15] JEON M, LEE J H, WOO T K, KIM S. Effect of welding and post-weld heat treatment on tensile properties of Nimonic 263 at room and elevated temperatures [J]. Metallurgical and Materials Transactions A, 2011, 42(4): 974−985.

[16] LIU C H, LAI Y X, CHEN J H, TAO G H, LIU L M, MA P P, WU C L. Natural-aging-induced reversal of the precipitation pathways in an Al−Mg−Si alloy [J]. Scripta Materialia, 2016, 115: 150−154.

[17] POGATSCHER S, ANTREKOWITSCH H, LEITNER H, EBNER T, UGGOWITZER G G. Mechanisms controlling the artificial aging of Al−Mg−Si alloys [J]. Acta Materialia, 2011, 59(9): 3352−3363.

[18] MARIOARA C D, ANDERSEN S J, JANSEN J, ZANDBERGEN H W. The influence of temperature and storage time at RT on nucleation of the β'' phase in a 6082 Al−Mg−Si alloy [J]. Acta Materialia, 2003, 51(3): 789−796.

[19] KUMAR N, JAYAGANTHAN R, BROKMEIER H G. Effect of deformation temperature on precipitation, microstructural evolution, mechanical and corrosion behavior of 6082 Al alloy [J]. Transactions of Nonferrous Metals Society of China, 2017, 27(3): 475−492.

[20] WANG F F, MENG W, ZHANG H W, HAN Z Q. Effects of under-aging treatment on microstructure and mechanical properties of squeeze-cast Al−Zn−Mg−Cu alloy [J]. Transactions of Nonferrous Metals Society of China, 2018, 28(10): 1920−1927.

[21] KHALFALLAH A, RAHO A A, AMZERT S, DJEMLI A. Precipitation kinetics of GP zones, metastable η' phase and equilibrium η phase in Al−5.46wt.%Zn−1.67wt.%Mg alloy [J]. Transactions of Nonferrous Metals Society of China, 2019, 29(2): 233−241.

[22] LI J F, HUANG J, LIU D Y, CHEN Y, ZHANG X, MA P. Distribution and evolution of aging precipitates in Al−Cu−Li alloy with high Li concentration [J]. Transactions of Nonferrous Metals Society of China, 2019, 29(1): 15−24.

[23] YANG W, JI S, HUANG L, SHENG X, LI Z, WANG M. Initial precipitation and hardening mechanism during non-isothermal aging in an Al−Mg−Si−Cu 6005A alloy [J]. Materials Characterization, 2014, 94: 170−177.

[24] EDWARDS G A, STILLER G A, DUNLOP G L, COUPER M J. The precipitation sequence in Al−Mg−Si alloys [J]. Acta Materialia,

1998, 46(11): 3893−3904.
[25] CHROMINSKI W, LEWANOWSKA M. Precipitation phenomena in ultrafine grained Al−Mg−Si alloy with heterogeneous microstructure [J]. Acta Materialia, 2016, 103: 547−557.
[26] YU H, WANG M, JIA Y, XIAO Z, CHEN C, LEI Q, LI Z, CHEN W, ZHANG H, WANG Y, CAI C. High strength and large ductility in spray-deposited Al−Zn−Mg−Cu alloys [J]. Journal of Alloys and Compounds, 2014, 601: 120−125.
[27] WANG Y, ZHANG G, XU X, CHEN X, ZHANG W. Microstructures and mechanical properties of spray deposited 2195 Al−Cu−Li alloy through thermo-mechanical processing [J]. Materials Science and Engineering A, 2018, 727: 78−89.

焊后热处理对 6061-T6 铝合金焊接接头组织和力学性能的影响

易 杰[1,2]，王 冠[2]，李世康[3]，刘志文[4]，龚艳丽[1]

1. 湖南工业职业技术学院 机械工程学院，长沙 410208；
2. 湖南大学 汽车车身先进设计制造国家重点实验，长沙 410082；
3. 湖州师范学院 求真学院，湖州 313000；
4. 南华大学 机械工程学院，衡阳 421001

摘 要：通过扫描电镜和透射电镜研究焊后热处理时间和温度对 6061 铝合金双脉冲 MIG 焊接接头显微组织的影响。采用硬度测试和拉伸实验研究热处理时间和温度对 6061 铝合金双脉冲 MIG 焊接接头力学性能的影响。结果显示，时效时间和温度对显微硬度的影响较大。增加时效温度有助于缩短峰值时效时间。未时效状态下，焊接接头内部存在许多位错和少量析出相组织。随着时效温度和时间的增加，接头处位错密度逐渐降低，同时，沉淀相逐渐析出并长大。当时效温度增加至 200 °C 时，焊接接头处析出较大的 Q'相，此时焊合接头的硬度达到最大。

关键词：6061 铝合金；双脉冲 MIG 焊；焊后热处理；组织演变；力学性能

(Edited by Xiang-qun LI)